

A spectral differential approach to characterizing low-mass companions to late-type stars

N.M. Kostogryz^{1,2,3,*}, M. Kürster², T.M. Yakobchuk¹, Y. Lyubchik¹, and M.K. Kuznetsov¹

¹ Main Astronomical Observatory of NAS of Ukraine (MAO NASU), Zabolotnoho 27, 03680, Kyiv, Ukraine

² Max Planck Institute for Astronomy, Königstuhl 17 D-69117 Heidelberg, Germany

³ Kiepenheuer-Institut für Sonnenphysik, Schöneckstr.6, D-79104 Freiburg, Germany

Received 28 August 2012

Published online later

Key words (stars:) binaries: spectroscopic, stars: late-type, stars: low-mass, brown dwarfs

In this paper, we develop a spectral differential technique with which the dynamical mass of low-mass companions can be found. This method aims at discovering close companions to late-type stars by removing the stellar spectrum through a subtraction of spectra obtained at different orbital phases and discovering the companion spectrum in the difference spectrum in which the companion lines appear twice (positive and negative signal). The resulting radial velocity difference of these two signals provides the true mass of the companion, if the orbital solution for the radial velocities of the primary is known. We select the CO line region in the K-band for our study, because it provides a favourable star-to-companion brightness ratio for our test case GJ1046, an M2V dwarf with a low-mass companion that most likely is a brown dwarf. Furthermore, these lines remain largely unblended in the difference spectrum so that the radial velocity amplitude of the companion can be measured directly. Only if the companion rotates rapidly and has a small radial velocity due to a high mass, does blending occur for all lines so that our approach fails. We also consider activity of the host star, and show that the companion difference flux can be expected to have larger variations than the residual signal from the active star so that stellar activity does not inhibit the determination of the companion mass. In addition to determining the companion mass, we restore the single companion spectrum from the difference spectrum using singular value decomposition.

© WILEY-VCH Verlag GmbH & Co. KGaA, Weinheim

1 Introduction

A large number of substellar companions to normal stars have been found to date, and substantial effort is devoted by the astronomical community to determine the characteristics of these objects. The most successful technique for the discovery of such objects is the radial velocity (RV) method. Unfortunately, it leads to a rather limited knowledge of a detected companion. A precise determination of the mass of the companion object is not possible unless the data can be combined with observations obtained with other techniques (e.g. transits or astrometry) or constrained by the dynamical interaction effects occurring in multi-planet systems. The radial velocity method alone can only provide a minimum mass that, even though it is also the most probable mass, cannot by itself provide an unambiguous decision about the true nature of the companion object. Therefore, it is very important to develop new approaches to characterising low-mass companions to stars that provide a dynamical mass of the companion object.

The present paper introduces a spectral differential method to the suite of techniques with which the dynamical mass and therefore the true nature of low-mass companions can be established. We develop our technique around

the example of GJ1046b, which is a companion to the inactive old M2.5V star GJ1046 that was found by Kürster et al. (2008; see also Zechmeister et al. 2009) in their M dwarf RV program with the Ultraviolet and Visual Echelle Spectrograph (UVES) at the ESO VLT. This object has a minimum mass of 27 Jupiter mas (M_{Jup}) that was derived from RV measurements. From a combination of the radial velocity measurements with Hipparcos astrometry (Kürster et al. 2008) determined a confidence of 97% that the companion is a brown dwarf (i.e. a chance probability of just 3% that it exceeds the stellar mass threshold). With a separation of 0.42 AU the companion is close to its host star and consequently it is located in the so called brown dwarf desert region. The orbital period is 168.8 d, the RV semi-amplitude is 1.83 km s^{-1} . The orbit is moderately eccentric with an eccentricity of 0.28.

The brown dwarf desert is an observational range of orbits around a star in which brown dwarf companions are very rare (Klahr & Brandner 2006, Grether & Lineweaver 2006). Its existence has been identified for typical star-companion separations of up to ~ 5 AU. The origin of the brown dwarf desert is currently not fully understood and subject of a considerable amount of research (Stamatellos & Whitworth 2009). What its existence seems to indicate is that two distinctive formation mechanisms are at work for planetary and stellar companions with relatively little

* Corresponding author: e-mail: kosn@mao.kiev.ua

overlap between the two. At wide separations (>1000 AU) no brown dwarf desert is observed. Originally defined for solar-type stars the brown dwarf desert is now also known to exist for early M dwarfs due to the small number of close-in brown dwarf companions to these stars. But as the mass ratios of binary systems with low-mass primaries tend towards unity, brown dwarf companions to late M dwarfs become more frequent (Montagnier et al. 2006).

Around solar-type stars, few brown dwarf companion candidates in the separation regime up to a few AU are known. The first such candidate was HD 114762 (Latham et al. 1989, Cochran et al. 1991, Mazeh et al. 1996), followed by HD 168443c (Marcy et al. 2001), HD 202206b (Udry et al. 2002), HD 137510 (Endl et al. 2004), HD 191760 (Jenkins et al. 2009) and others. A transiting brown dwarf has also been discovered by the CoRoT spacecraft. This object, CoRoT-Exo-3b, has a mass of $21.7 M_{\text{Jup}}$ and a radius of 1.01 Jupiter radii (R_{Jup}), in a remarkably close orbit at 0.05 AU (Deleuil et al. 2008). The most recent brown dwarf companion in the brown dwarf desert range is TYC 1240-00945-1 (Lee et al. 2011). As will be pointed out in Section 3, the star-to-companion brightness contrast is an important parameter for our technique. For the mentioned objects this contrast is very large.

A more favourable brightness contrast can be found in systems comprised of a brown dwarf orbiting an M-type star in the brown dwarf desert range. Such objects can typically be found with RV measurements. There are several known candidates for probable brown dwarf companions to M-type stars, such as GJ1046 (Kürster et al. 2008), GJ595, GJ623, and GJ84 (Nidever et al. 2002).

For this paper we chose GJ1046 as a sample to develop our technique, but certainly, we can apply this method to other brown dwarf companions to M-type stars.

2 Synthetic spectra

We computed synthetic spectra for M dwarfs and brown dwarfs using the WITA612 programme (Pavlenko 2000a). All calculations were carried out under the assumption of local thermodynamic equilibrium, hydrostatic equilibrium, and absence of sources and sinks of energy. The solar abundances reported by Anders & Grevesse (1989) were used in the calculations. All details of the other input parameters are described by Pavlenko et al. (2000b).

A grid of synthetic spectra was computed from model structures of AMES-cond and AMES-dusty (Allard et al. 2001) for the following range of parameters: temperatures of 1500 K, 2000 K, 2500 K and 3500 K, $\log g = 5.0$, microturbulent velocity 2 km s^{-1} and solar metallicity.

The atomic line list used for the computation of synthetic spectra is taken from the Vienna Atomic Line Database (VALD; Kupka et al. 1999). The main contributors of the molecular absorption around $\sim 2.3 \mu\text{m}$ are water and carbon oxide. In our computations we used line lists

BT2 for H_2O by Barber et al. (2006) and CO by Goorvitch (1994).

All theoretical spectra were computed with a wavelength step of 0.01 \AA and convolved with a Gaussian profile to match the spectral resolution of the instrument to be used for the observations. Rotational broadening of spectral lines is implemented by convolution with a rotational profile following Gray (1976):

$$G(\Delta\lambda) = (2(1 - \epsilon)[1 - (\Delta\lambda/\Delta\lambda_L)^2]^{1/2} + 0.5\pi\epsilon[1 - (\Delta\lambda/\Delta\lambda_L)^2]) / (\pi\Delta\lambda_L(1 - \epsilon/3)) \quad (1)$$

where $\Delta\lambda_L = (\lambda v \sin i)/c$, ϵ is the limb darkening coefficient. Typically for our computations we have adopted a value of 0.6 which is sufficiently close to the K-band value for ultra-cool companions of 1500 K - 2500 K (Claret & Bloemen 2011), and the dependence on this value is very small.

3 Method of difference spectrum

Our method aims at discovering companions to late-type stars by removing the stellar spectrum through subtraction of spectra obtained at different orbital phases and identifying the companion spectrum in the difference spectrum. Using near-infrared spectra of sufficient resolution one can attempt to search for absorption lines of the companion in the spectrum. In our approach we take one spectrum each near the maximum and the minimum of the radial velocity curve of the star, shift them in wavelength in such a way that the stellar line systems co-align and subtract them from each other thereby removing the stellar signal (not the photon noise, of course, that still has to be dealt with). What one is left with is a spectrum that consists of the difference of two spectra of the companion, but taken at different radial velocities. The companion lines will therefore appear twice in this difference spectrum, once as a positive signal and once as a negative signal. By determining the radial velocity difference of these two signals one can obtain the star-to-companion mass ratio and, if the stellar mass is known, one can determine the true mass of the companion and thereby its nature.

The spectrum of the invisible companion will be detected when the star-to-companion brightness ratio (hereafter called "the contrast") of the two components of the system is sufficiently small. The smaller the contrast, the higher the probability to detect cool companions. Obviously, the best wavelength range for low-mass star observations is the near-infrared (NIR). Knapp et al. (2004) provide the absolute magnitude - spectral type dependence in the J and K bands for objects from L0 to T9, from which we infer that in the J band the contrast is less favourable for spectral types L0-T0 than in the K band while the contrast of late T dwarf companions relative to GJ 1046 is smaller in the J-band than in the K-band. Figure 1 shows the J and K band flux ratios of various field brown dwarfs as they would

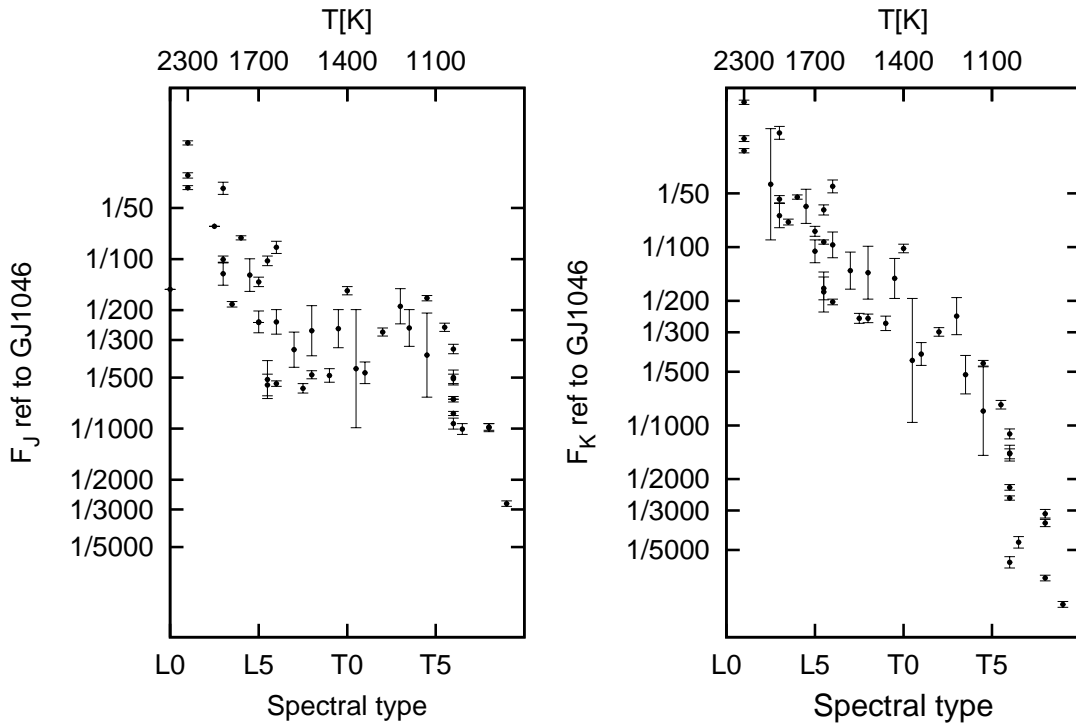


Fig. 1 The J and K band flux ratios relative to GJ 1046 of field brown dwarfs with spectral types from L0 to T9. Temperature values (upper x-axis) that correspond to the different spectral types were taken from Testi (2009).

be observed at the distance of GJ 1046 with spectral types between L1 and T8 and corresponding temperatures (Testi 2009). The data were taken from Knapp et al. (2004).

To realize our approach, observations should be made at two epochs with different stellar radial velocities. In order to resolve the spectral features we plan to study we need an NIR spectrograph with high resolution of the order 50,000 - 100,000. The most suitable instrument for this technique is the cryogenic high-resolution infrared spectrograph (CRIRES) that is mounted at the Very Large Telescope of the European South Observatory.

The absence of high-resolution spectroscopic observational data for GJ1046 leads us to simulate CRIRES observations in order to investigate the feasibility for the detection of the companion in the difference spectrum. For this purpose we take the synthetic spectra described in Section 2. As we do not know the spectral type of the companion, we take spectra with effective temperatures of 1500 K, 2000 K and 2500 K as samples to find out which of them can be detected. All these spectra were convolved with Gaussian instrumental profiles whose width can be chosen to match the

resolution and spectral sampling of different instruments. Using cubic spline interpolation we map all these spectra to a sampling grid representing that of CRIRES.

The selection of the spectral range is important for our approach. Depending on the system, one needs to choose a wavelength range with small contrast and narrow lines. Since they are strong features, we have first considered the KI doublets in the J band but then we rejected them because their widths lead to blending problems (see below). The strong KI doublet lines in the J band become self-superimposed in the difference spectrum. Blending leads to an apparent increase of the wavelength shift and underestimation of the companion mass.

Therefore, in our approach we switched to longer wavelengths (K band), which is preferable in order to do away with the blending problem and, besides that, having better contrast and signal-to-noise ratio.

Also, the narrow spectral lines of the CO molecule are prominent throughout spectral types late-M to T in K band. We choose the CRIRES wavelength range order 24, standard settings, reference wavelength

2.3252 μm (see the CRIRES User's Manual, [http : //www.eso.org/ rsiebenm/crires](http://www.eso.org/rsiebenm/crires)) because it allows us to observe CO lines in the inner two detectors. Note that the outer two detectors of CRIRES provide a short wavelength coverage. Figures 2-5 are presented in this CRIRES wavelength range. The synthetic spectra of the host star and companion are presented in Figure 2. For the chosen spectra of effective temperatures 2500 K, 2000 K and 1500 K the absolute flux ratios in K band are 1/20, 1/60 and 1/250, respectively (see Fig.1).

As is seen from Fig. 2 the CO lines are contaminated by telluric absorption lines which must be divided out from the observational spectrum using synthetic telluric spectra (Clough et al. 1992, Clough et al. 1995, Clough et al. 2005, Rothman et al. 2009, Seifahrt et al. 2010).

We assume that the orbital solution for the primary is well known from optical radial velocity data so that the RV of the primary can be predicted for both spectra. The uncertainties of the orbital solution of the primary are very small and do not affect the results derived with the technique presented here (see Section 4). Provided that a perfect correction can be achieved for the stellar radial velocity difference between the two spectra to be subtracted from each other, which includes also a correction of the barycentric motion of the Earth, we can assume that the stellar spectrum cancels (see, however, Section 4). Another possible way to achieve the removal of the stellar spectrum would consist of aligning the two spectra via cross-correlation and then subtracting them from each other. However, the stellar spectra are contaminated to an unknown amount by the companion signal which may affect the result of the cross-correlation and make this approach unreliable, so that we do not follow it. For the purpose of our simulations it suffices then to subtract the companion flux $f(\lambda_i)$ from flux $f(\lambda_{i+\Delta i})$, which is shifted in wavelength by an amount $\Delta\lambda$ approximated by the nearest-integer shift in pixels Δi . The value of $\Delta\lambda$ can be calculated according to the Doppler formula as

$$\Delta\lambda = \frac{\Delta RV M_1}{c M_2} \lambda \quad (2)$$

where ΔRV is the RV difference of the host star at the two different epochs and equal to twice the RV semi-amplitude of the star, $2K_1$, when one observes at the extrema, M_1 is the host star mass, M_2 is the companion mass.

Consequently, the difference spectrum is calculated using the equation:

$$df(\lambda_i) = f(\lambda_i) - f(\lambda_{i+\Delta i}) \quad (3)$$

We generate Poisson distributed photon noise with a signal-to-noise ratio (SNR) equal to 500 per spectral pixel for each of the spectra from the different observational epochs. When taking the difference of the two spectra the photon noise is propagated accordingly.

Having obtained the input model difference spectrum (see below Fig.8) we can proceed to the procedure that simulates the companion mass determination. Practically, it consists of an accurate determination of the wavelength

shift. In the absence of blending the spectral shift can be found as the simple positional difference between the positive and negative peaks averaged over all lines.

Overall, the procedure was performed as follows. First, we determine an initial guess shift value as the most frequent from visual inspection of all features. Then we register all line peaks that exceed a selected positive or negative intensity threshold. Then we filter out unpaired peaks, paired peaks with intensity difference larger than the value adopted as initial guess and those with separation beyond the adopted shift range (adopted value ± 0.5). An additional check can be done visually to remove lines with bad or blended profiles (Fig.3). Finally, having selected a suitable set of lines we can find the average spectral shift Δi_{out} , its errors and the corresponding companion mass value M_{out} and error. Based on our model difference spectra we find that the presented procedure is successful enough to recover the input companion mass (see below Table 1).

4 Host star M2.5V dwarf

In this section we consider the impact of uncertainties related to the primary star on the results derived with our spectral differential technique.

4.1 Misalignment due to wavelength calibration errors

Apart from the blending issue, we consider that the largest source of systematic error is likely to come from errors in the wavelength calibration leading to imperfect alignment of the shifted stellar spectra before they get subtracted from each other. We therefore simulated the residual host star spectral features that would arise from this mismatch. As input spectrum for the M2.5V host star we use a synthetic spectrum for a temperature of 3500 K.

We introduce shift values of 1.0, 0.5, 0.1, and 0.05 pixels before subtracting the spectrum from the so shifted version of itself. For the worst case of a non-transiting star (see below) Figure 4 shows the residuals and indicates the photon noise level. As can be seen from Figure 4, the difference spectrum for the host star is beneath the noise level. While considerably higher for shift values of 1.0 and 0.5 pixels, the height of the strongest peaks are only at 2.82 sigma for the 0.1 pixel shift value and at 1.39 sigma for 0.05 pixels. Therefore, during the data reduction one should aim to achieve wavelength calibration errors less than 0.1 pix. Using the telluric lines present in the spectra Brogi et al. (2012) obtained wavelength calibration errors of $0.15 - 0.20 \text{ km s}^{-1}$ for CRIRES in the same spectral region that we consider. As the pixel (px) width in CRIRES is equal to 1.5 km s^{-1} , the errors in the calibration are $0.1 - 0.13 \text{ px}$. These values are the upper limit for our technique, therefore, we plan to use all possible options for the wavelength calibration to achieve smaller errors. There are several other options

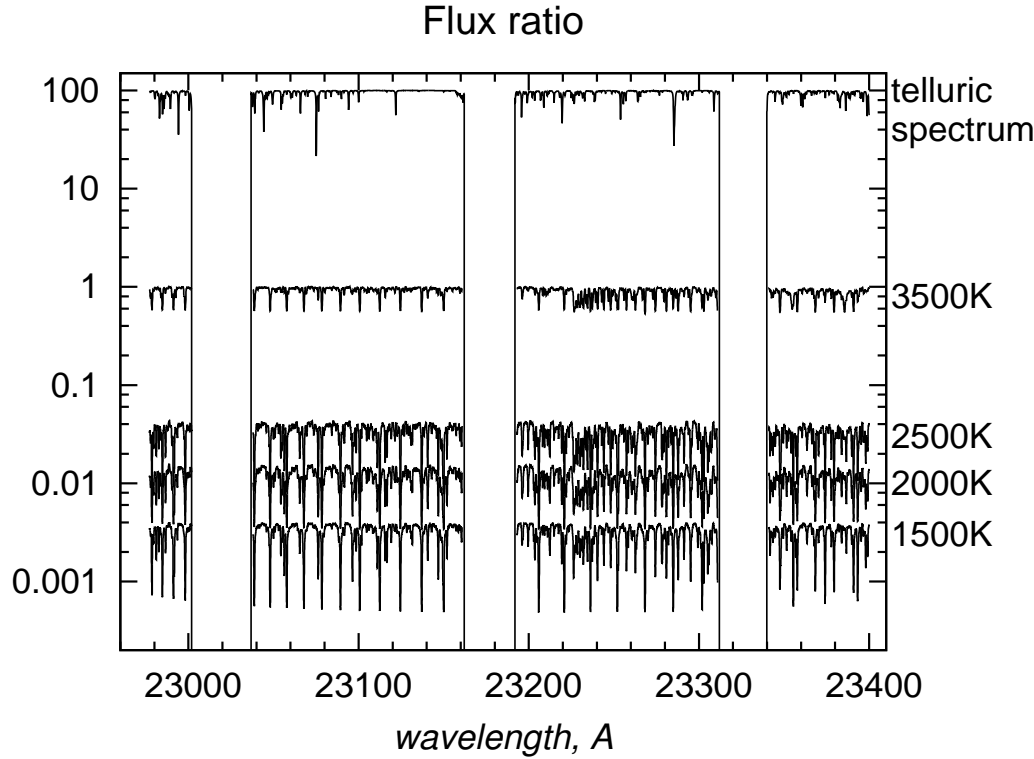


Fig. 2 NIR spectra for 3500 K, 2500 K, 2000 K and 1500 K effective temperature with their absolute flux corresponding to the mean contrast for field brown dwarfs (cf. Fig. 1). The upper spectrum is the transmission spectrum of the Earth's atmosphere taken from the CRIRES exposure time calculator (<http://www.eso.org/observing/etc/bin/gen/form?INS.MODE=lwspectr+INS.NAME=CRIREs>). The three gaps in the wavelength regime near $2.302\ \mu\text{m}$, $2.319\ \mu\text{m}$, and $2.332\ \mu\text{m}$ are due to physical gaps in the array of the four Aladdin detectors in CRIRES. Note also that due to vignetting the outer two detectors provide a shorter wavelength coverage than the inner two.

for the wavelength calibration in ESO's standard calibration plan like ThAr spectrum or an N_2O gas cell that can be used during spectra reduction.

4.2 Uncertainties in the orbital solution of the primary

Uncertainties in the parameters of the orbital solution can lead to systematic errors in the assumed radial velocity shift of the stellar spectrum. This can affect the precision with which the two stellar spectra (taken at two different orbital phases) can be aligned before they are subtracted from each other.

The true orbital phase may differ from the calculated one due to the error in the orbital period and due to the error in the periastron passage time. While the latter is constant and known, the former is also known but proportional to the number of orbital cycles elapsed between the time of observation and the epoch at which the ephemeris was determined.

According to Kürster et al. (2008) the orbital period for GJ1046 is $168.848 \pm 0.030\text{d}$ and the time of periastron $T_p = \text{BJD}2453225.78 \pm 0.32(\text{d})$. The ephemeris were determined at epoch 2006.0 while we are planning for observations for epoch 2014.0. The difference of the epochs is

equal to 8 yr, i.e. 2922 d, i.e. 17.31 orbital cycles. Considering this difference the accumulated phase error is 0.519 d. The combined uncertainty including the accumulated phase error and the error of the periastron time the maximum uncertainty is 0.61 d.

The maximum RV change (occurring on the descending branch of the RV curve where the RV is equal to the systemic RV which is actually an uninteresting phase for our technique) is $-0.125\text{kms}^{-1}\text{d}^{-1}$ (as can be inferred from Fig. 1 in Kürster et al. 2008), i.e. -0.0801pxd^{-1} as the pixel width for CRIRES is 1.56kms^{-1} . The uncertainty in the RV due to the error in phase is, therefore, less than 0.077kms^{-1} , i.e. $< 0.049\text{px}$ everywhere on the RV curve, and much less near the extremal values of the curve. For the difference of two observations this uncertainty will in most realistic observational scenarios be reduced further.

However, it can be increased when observing at the descending and ascending branches. So, the worst case is when observations are carried out near the systemic RV, where in the ascending branch a velocity up to $0.0399\text{kms}^{-1}\text{d}^{-1}$, i.e. 0.0256pxd^{-1} can be reached leading to an uncertainty of the phase of 0.0207kms^{-1} , i.e. 0.0133px (the uncertainty in the constant time of periastron passage is not included again). In this worst case the com-

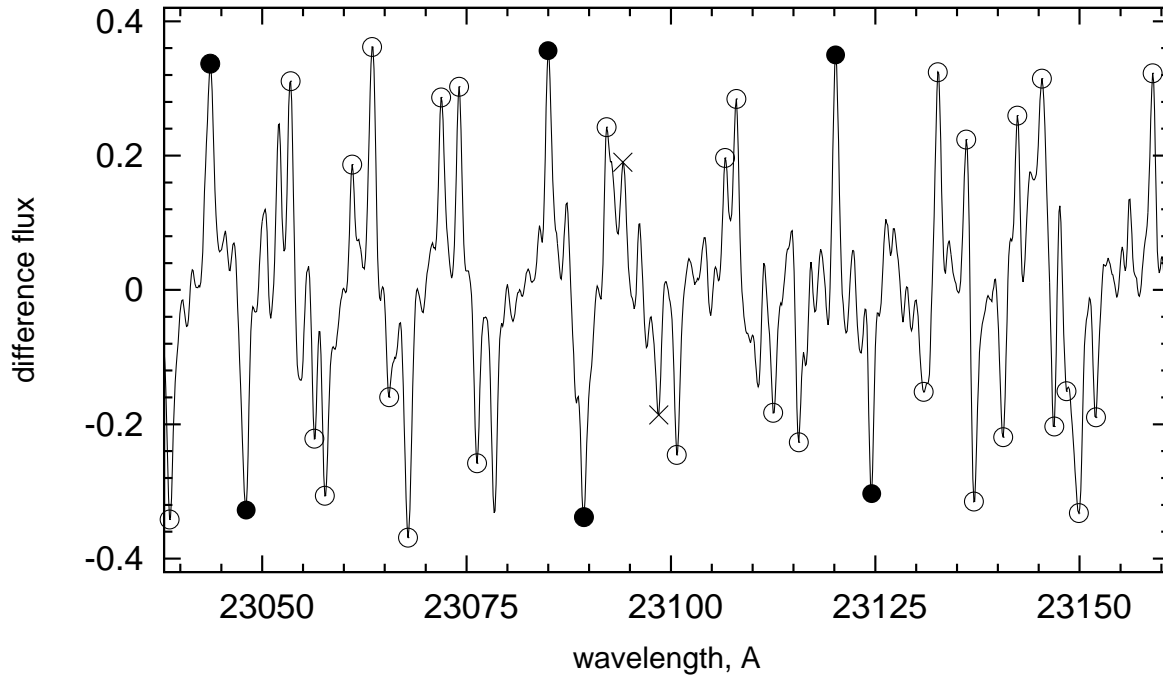


Fig. 3 Difference spectrum for a non-rotating companion with the minimum mass and 2500 K effective temperature. Shown is the spectral range from 23030 Å to 23160 Å that corresponds to the wavelength range of the second CRIRES detector. Open circles depict all automatically identified peaks that do not survive the filtering process (see Sect. 3). Crosses mark automatically identified peaks that do not survive the visual inspection. Filled circles indicate peaks that survive to the end.

binned uncertainty is then $< 0.080 \text{ km s}^{-1}$ or $< 0.051 \text{ px}$. As it is seen from Fig. 4 even in the worst case the uncertainties of the primary's orbital solution can be neglected in our technique. But the observations are planned at phases where the RV changes are expected to be much slower so that the uncertainties will also be much smaller.

4.3 Activity of the host star

Another source of systematic error in our approach could be the activity of the star, i.e. star spots. As we need to observe at different observational epochs our approach may be susceptible to changes in the stellar surface temperature distribution arising from appearing and disappearing star spots. The influence of stellar activity on the determination of the companion mass with our difference spectrum technique is the subject of a set of simulations presented in the following.

It is known from the Sun that magnetic activity can cause spots which are significantly cooler than the quiet photosphere. However, for very active stars the temperature difference of spots and photosphere remains a rather unknown parameter. According to Solanki (2003) the coolest temperature for sunspots is about 2000 K lower than for the photosphere. For active G- and K-type stars the spots can cover between 10% and 50% of the stellar surface and have

temperatures up to 1500 K below photosphere (O'Neal et al. 2001, O'Neal et al. 2004, Reiners et al. 2010).

From available observations, no information is available on spot distributions in M dwarfs, i.e. in stars with atmospheres that differ substantially from those of Sun-like stars. Therefore, we make the following type of simulations. We assume a single spot that is a function of

- spot surface filling factor;
- spot-to-photosphere temperature ratio;
- the instantaneous radial velocity of the spot on the rotating star.

In attempt to study worst case conditions we choose the spot geometries shown in Fig. 5. In the first example the star is spot free at one of the two observational epochs, whereas it is fully covered by the spot at other epoch (a). In this case there is a maximum difference between the two spectra of the star. In the two examples labelled (b) the spot filling factors of the visible hemisphere are $1/2$ and $1/3$, respectively. Assuming that the star rotates counterclockwise when viewed from above, then the spot is completely placed on the receding hemisphere and covers the location of the largest possible RV values in order to maximize RV shift effects between the spectra taken at the two epochs. In the two examples labelled (c) RV shift effects are increased even further due to the fact that the spots now appear at both epochs, but at mirror-symmetric locations.

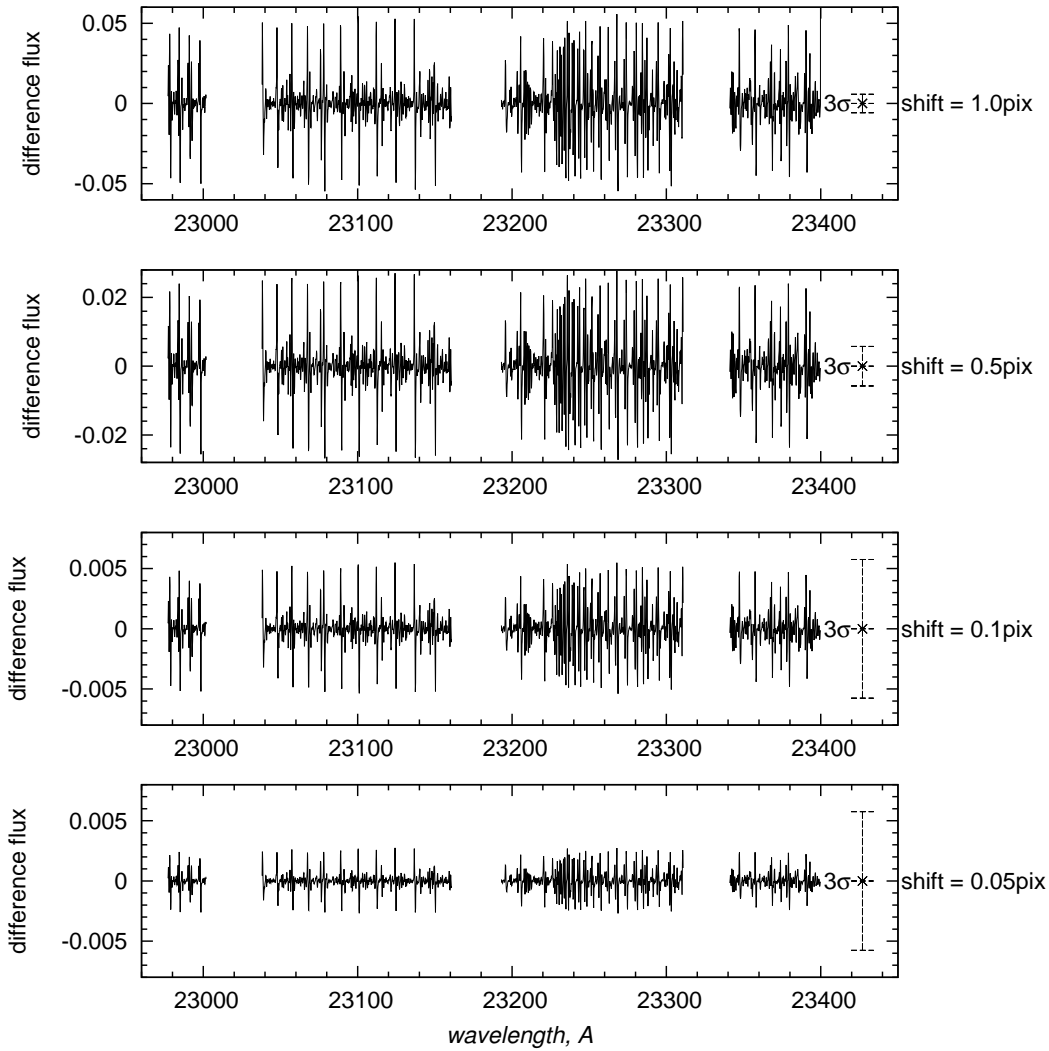


Fig. 4 Difference spectra for a non-rotating host star with a wavelength calibration mismatch of 1.0, 0.5, 0.1 and 0.05 pixels. Note that for display purposes the photon noise has not been added to the signal, but is indicated by the 3-sigma error bars near the right end of the panels.

Reliable spot temperature values for early M dwarfs are not available. In order to study worst case effects we therefore choose a spot temperature that is 1000 K below the photospheric temperature (Terndrup et al. 1999, Scholz et al. 2005, see also last paragraph of this section). The combined stellar spectrum is then composed by the spectrum of the unspotted photosphere and the spectrum of the considering the areas covered and the RV shifts.

Considering the rotation of the star, we have to shift the cooler spectrum relative to the hotter one in wavelength according to the assumed velocity that results from stellar rotation. Convolution of the cooler spectrum with that part of the rotational profile (Eq. 1) that corresponds to the spotted area, and the hotter spectrum with that part of the rotational profile that corresponds to the unspotted area of the star, adding these spectra and convolving the result with the instrumental profile of CRIRES, we obtain the spectrum of

the object during the individual epoch. The same procedure is applied to the second observational epoch. Then, taking a difference between the spectra from two epochs, we get the residual spectrum for the active star (Fig. 6). In Fig. 6 the first row is plotted for visible hemisphere spot filling factors of 1 and 1/2 and for the cases depicted in the first column of Fig. 5; the second row is the residual spectrum of the active host star corresponding to the second column in Fig. 5; in the third and fourth rows we show the difference flux of the companion with effective temperature 1500 K and for the minimum and maximum masses of the companion, respectively. The three columns of the Fig. 6 are for different rotational velocities of the star (first two rows) and the companion (last two rows), respectively. As star and companion do not necessarily have the same rotational velocity, one can compare the residual stellar and difference companion spectra for different rotational velocities. Fig. 6 shows that

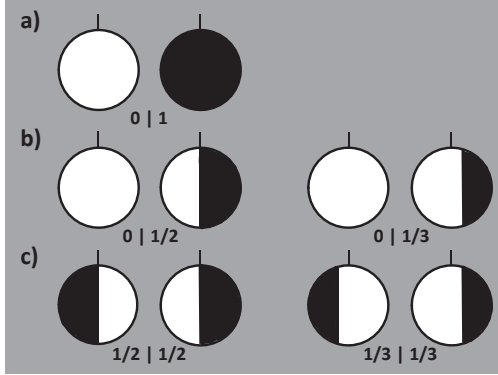


Fig. 5 Illustration of spot distributions on the host star that are considered in our simulations. In case (a) the spectra observed at different two epochs will maximally differ from each other. In cases (b) and (c) there will also be RV shifts between the pairs of spectra.

in extreme cases, such as those we are studying, differences in the overall spot coverage between the two observational epochs can be more important than RV shifts. For the given spot temperature the large spot coverage difference corresponding to configuration (a) in Fig. 5, leads to stronger variations in the difference spectrum than RV shifts between spot and photosphere (configurations b and c), because latter can only be produced by a partial spot coverage. As is seen from Fig. 6 we can neglect the activity of the star except in the most extreme case when we have a slowly rotating and a spotless star during the first epoch and completely spotted star during the next observational epoch (Fig. 6, top left panel, curve labelled "a"), and fast rotation and maximum mass for the companion (Fig. 6, bottom right panel).

However, the spot-to-photosphere brightness ratio is smaller in the NIR (Tendrup et al. 1999, Scholz et al. 2005). For this worst case, i.e. maximum variations in the host star difference spectrum and minimum variations for the companion difference spectrum, we now study the effect of reducing the temperature difference between spot and photosphere to values in the range of 100 K to 500 K. We simulate the residuals from the extremely active host star (Fig. 5, a) that rotates with $v \sin i = 5 \text{ km s}^{-1}$ and the difference flux of the fast rotating ($v \sin i = 20 \text{ km s}^{-1}$) companion that has maximum mass (Fig. 7). In Fig. 7 the thick solid line corresponds to the companion difference spectrum and the thin solid lines depict the residual signal from the host star for the considered temperature differences. So, when the temperature difference of the star between the two epochs is 500 K, the activity could still be a problem for our technique, but it should be mentioned here that this case is quite unrealistic. If the star is so active that half of its surface is covered by a cool spot, it should rotate very fast which lead to broadening of its spectral lines and will result in a decreasing of the variations in the residual spectrum (see Fig. 6). And moreover, even for such an extreme case, the activity of the host star is not an issue any more for our tech-

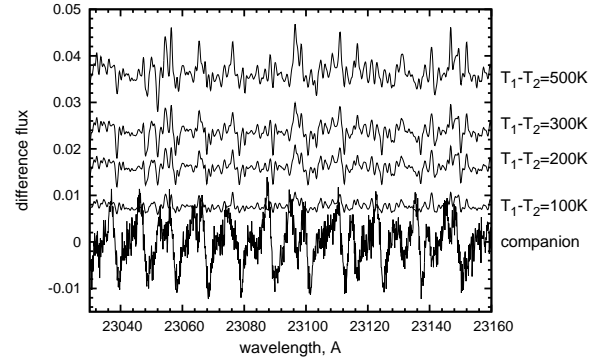


Fig. 7 Simulation of the residual signal of the active star that has small rotational velocity ($v \sin i = 5 \text{ km s}^{-1}$) and is very active (the geometry of the spot corresponds to the case "a") (Fig. 5) (thin lines) compared to difference flux of the companion with the maximum mass and rotational velocity of 20 km s^{-1} (thick line). The labels point at the temperature differences of the host star between the two observational epochs.

nique when the temperature difference is smaller than 500 K. As was shown by Tendrup et al. (1999), for a star with a mass similar to that of GJ1046 the temperature contrast in the NIR is about 6%, i.e. 200 K but the spot-filling factor is only 13% that is smaller than in our simulation. So, the activity of the star should not be an issue in our technique.

5 Companion brown dwarf

By planning for observations of GJ1046 near the minimum and maximum of its RV curve and then subtracting the obtained spectra from each other we aim at the discovery of the CO lines of the brown dwarf candidate companion to the M2.5V host star.

Figure 8 presents simulations of difference spectra taken at maximum and minimum companion RV, previously shifted to correct for stellar orbital and Earth's barycentric motions thereby making the stellar spectrum cancel.

In the difference spectrum the most interesting structures are the combined absorption/pseudoemission features produced by each of the absorption lines resulting from the wavelength shift between the two spectra of the companion. The observed signature at the CO line positions is stronger for brighter companions. Note that even though the host star spectrum cancels, we are still left with the combined photon noise from the individual stellar spectra.

Experience with infrared detectors shows that very high signal-to-noise ratios (SNR) are difficult to achieve, because of several effects. The first such effect is the required high quality of flat-fielding in order to calibrate the strong pixel-to-pixel variations that these detectors have. The flat-fields provided by the CRİRES calibration plan for our selected wavelength setting possess an SNR ranging from about 1000 - 1400 per spectral bin (see [http : //www.eso.org/observing/dfo/quality/ALL/refra](http://www.eso.org/observing/dfo/quality/ALL/refra)

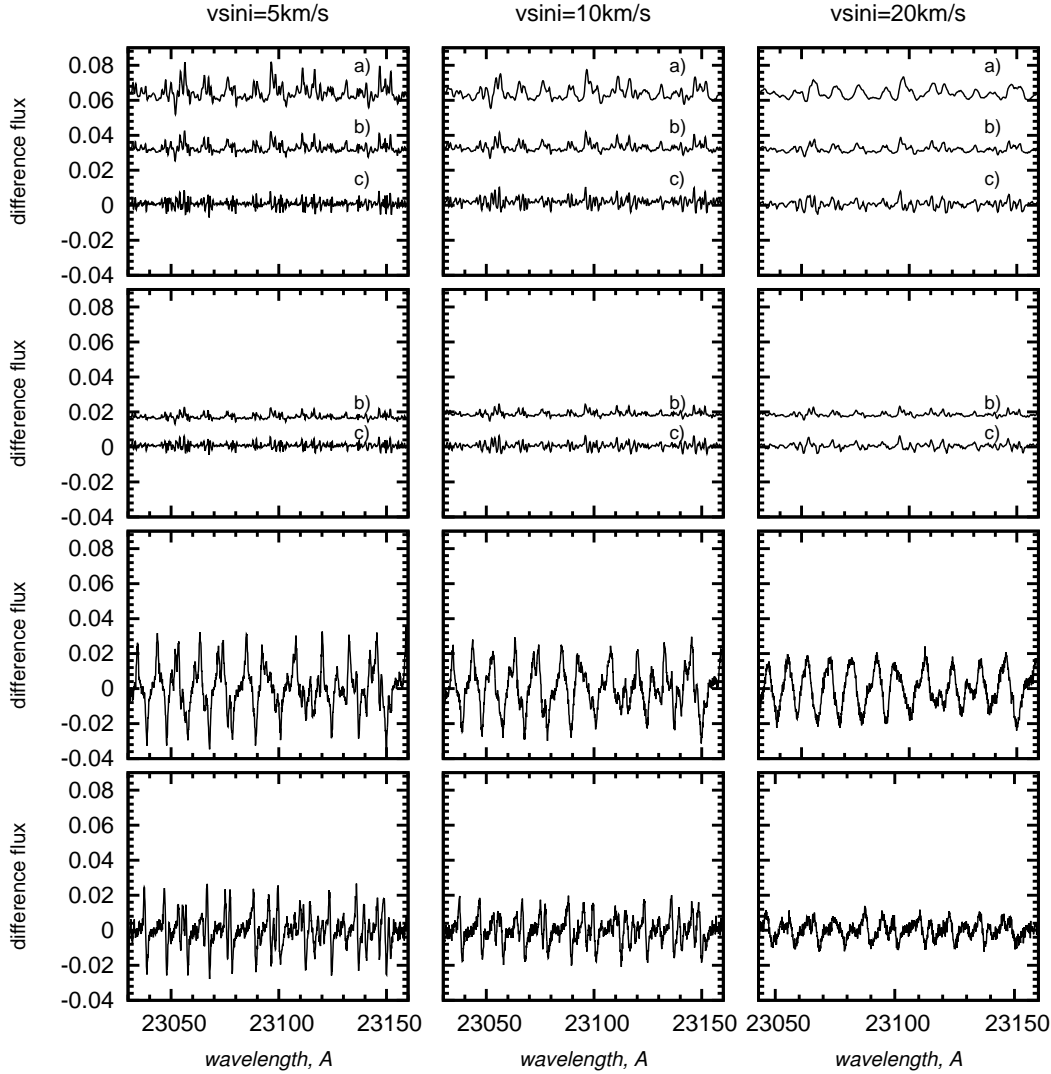


Fig. 6 Simulations of the residual signal from the active host star (upper two rows of panels) and the difference flux of the companion (lower two rows of panels) with an effective temperature of 1500K for different rotational velocities. The first row corresponds to the first column of Fig. 5. The second row presents the results of the simulation when the filling factor is equal to $1/3$ (second column of Fig. 5). The labels "a)", "b)", "c)" to the geometry shown in Fig. 5. The next two rows show the difference spectra of the companion with the minimum and the maximum masses, respectively. The signal in the companion difference spectrum exceeds that produced by the activity effects in the host star in almost all cases.

$mes/CRIRES/flat_{sn}/$). A second effect is detector non-linearities that effectively reduce the achievable SNR. They are a concern for the CRIRES Aladdin III detectors. Additionally, the quality with which the telluric lines can be removed or modelled will also influence the achievable SNR. These considerations lead us to assume (perhaps somewhat optimistically) that the maximum achievable S/N ratio with CRIRES will be about 500 per spectral bin, a value comparable to that attained also in other work, e.g. (Rodler et al. (2012)) who obtained an SNR of 300 at the same wavelength setting also for high-precision work.

Taking a signal-to-noise ratio of 500, we determine the difference spectrum for the three cases of the companion with effective temperatures 2500K, 2000K, 1500K (Fig. 8

shows this for the minimum mass but the result for maximum mass is very similar). As is seen from Figure 8, the signal to noise ratio is high even for the object with effective temperature 1500K. Therefore, we can confirm that it is feasible to detect this difference companion spectrum in the planned observations with CRIRES. Moreover, the object with a temperature of 1500K is not the lower limit for detecting the companion so that cooler object can also be detected in the difference spectrum.

Once we have obtained the difference spectrum, we will try to find the mass of the companion. For this purpose it is important to consider the broadening of the spectral lines due to rotation of the companion. The faster the rotation of the companion, the broader the CO lines will be and

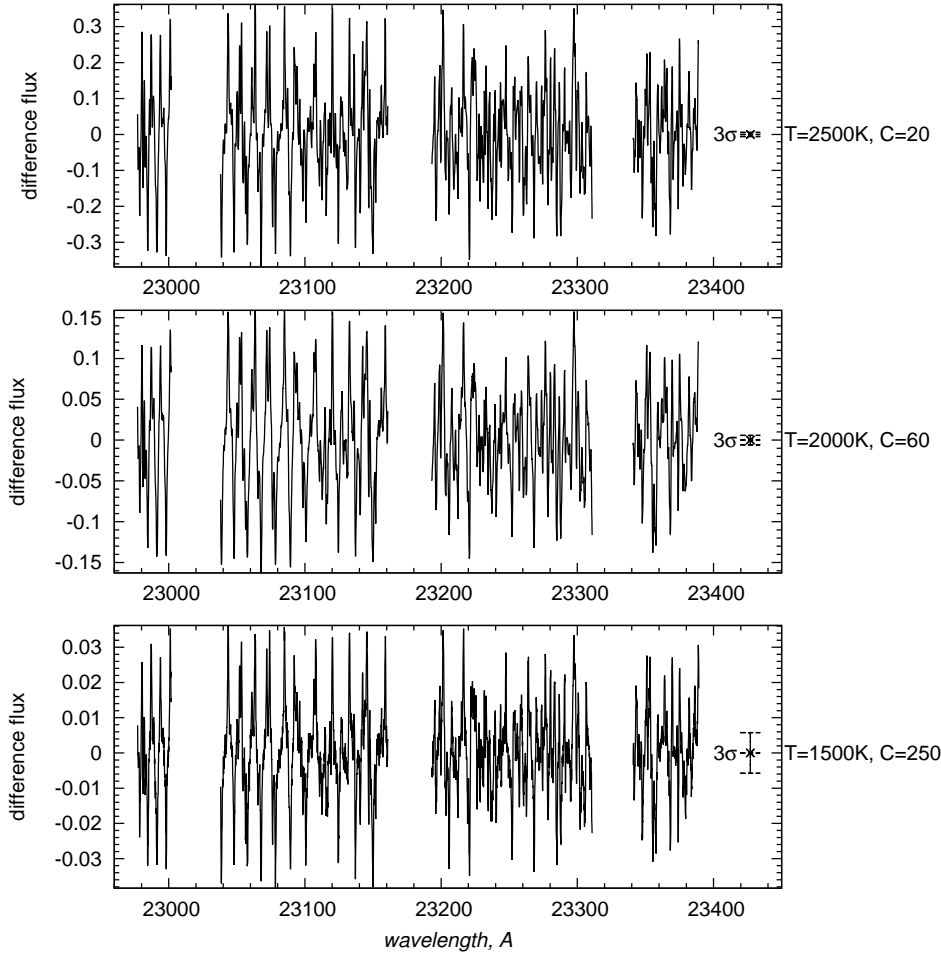


Fig. 8 Simulated difference spectra obtained from observations at companion's RV maximum and minimum. The stellar spectrum cancels. Three panels for effective temperatures 2500 K, 2000 K and 1500 K, and contrasts $C=20, 60, 250$, respectively, for the minimum possible companion mass $m_{2,min} = 26.85 M_{Jup}$. The solid line is the companion difference flux with photon noise added, the crosses together with the 3-sigma error bars depict just the photon noise.

therefore more blended lines will appear in the difference spectrum. All our synthetic spectra were convolved with a rotational profile corresponding to projected rotational velocities of 2 km s^{-1} , 5 km s^{-1} , 10 km s^{-1} , 15 km s^{-1} and 20 km s^{-1} to study how rotation of the companion influences the determination of the companion mass. The input values of the wavelength shifts and masses were taken from the difference spectrum as described in section 3 last paragraph. Then, we are looking for similar ($\Delta i_{in} \pm 0.5$) shifts between the pseudoemission and absorption in the difference spectrum. Because of the photon noise in the difference spectrum the obtained wavelength shifts may not correspond to the true ones. Therefore, after identifying the correct features in the difference spectrum we fit double Gaussians to the positive and negative peaks of the difference spectrum features using the Levenberg-Marquardt method from Numerical Recipes (Press et al. (1992), Marquardt 1963).

Table 1 shows the determined RV shifts and masses from the difference companion spectrum with various ro-

tational velocities. For a companion with the minimum possible mass no blending effect occurs in the difference spectra which results in a correct mass determination (Table 1) for all adopted rotational velocities. But, for the maximum companion mass it is only possible for rotational velocities of 2 km s^{-1} and 5 km s^{-1} , to find the correct wavelength shift and therefore the mass of the companion (all obtained masses are within $\sim 3 \sigma$ of the true mass). For higher rotational velocities, the obtained masses are wrong because of blending of the CO-lines in the difference spectrum (see Fig. 9).

6 Companion spectrum reconstruction

To reconstruct the (single) companion spectrum from the difference spectrum, we apply the method of singular value decomposition using the algorithm by Press et al. (1992) on difference spectrum. Using the shift value taken from Table 1, we reconstruct the single companion spectrum from the

Table 1 Determined companion masses for different rotational velocities of the companion: 2 kms⁻¹, 5 kms⁻¹, 10 kms⁻¹, 15 kms⁻¹ and 20 kms⁻¹. Input shift value in pixels Δi_{in} were taken from the difference spectra.

$v \sin i$	Δi_{in}	M_{in} (M_{Jup})	Δi_{out}			$M_{out}(M_{Jup})$		
			2500K	2000K	1500K	2500K	2000K	1500K
2	4.35	26.85	4.345±0.028	4.331±0.041	4.323±0.029	27.00±0.17	27.09±0.26	27.13±0.18
5	4.35	26.85	4.327±0.035	4.355±0.052	4.332±0.022	27.11±0.22	26.93±0.32	27.08±0.14
10	4.35	26.85	4.345±0.045	4.410±0.081	4.403±0.045	27.00±0.28	26.60±0.49	26.65±0.27
15	4.35	26.85	4.295±0.061	4.435±0.098	4.370±0.067	26.80±0.35	26.45±0.58	26.85±0.41
20	4.35	26.85	4.359±0.095	4.399±0.077	4.383±0.039	26.91±0.58	26.67±0.47	26.76±0.24
2	1.05	111.74	1.072±0.014	1.083±0.015	1.077±0.014	109.4±1.4	108.3±1.6	108.9±1.4
5	1.05	111.74	1.089±0.013	1.097±0.040	1.067±0.018	107.7±1.3	107.0±4.0	110.0±1.9
10	1.35	86.91	1.369±0.028	1.399±0.022	1.333±0.037	85.7±1.8	83.9±1.3	88.0±2.5
15	1.75	67.04	1.819±0.025	1.778±0.016	1.644±0.043	64.49±0.89	65.98±0.60	71.3±1.9
20	2.15	54.57	2.152±0.057	2.088±0.089	2.091±0.039	54.5±1.4	56.2±2.4	56.1±1.1

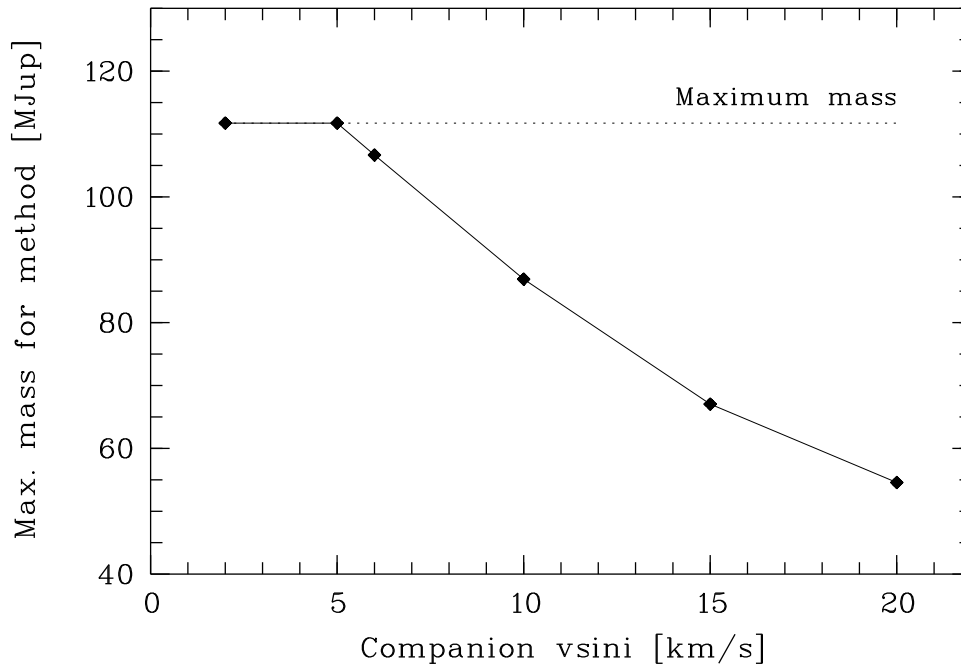


Fig. 9 Maximum value of the companion mass for which our difference spectrum approach yields a correct mass determination as a function of the $v \sin i$ of the companion (solid line with diamonds). The dotted line depicts the correct maximum mass value. Due to line blending the determination of masses in the regime between the two lines will yield values that are systematically too small.

difference spectrum. For each pixels we rewrite the system of equations (Eq.2) as the matrix equation:

$$\begin{bmatrix} df_1 \\ df_2 \\ \vdots \\ df_N \end{bmatrix} = \begin{bmatrix} A_{11} & A_{12} & \cdots & A_{1M} \\ A_{21} & A_{22} & \cdots & A_{2M} \\ \vdots & \vdots & \ddots & \vdots \\ A_{N1} & A_{N2} & \cdots & A_{NM} \end{bmatrix} \times \begin{bmatrix} f_1 \\ f_2 \\ \vdots \\ f_N \end{bmatrix} \quad (4)$$

where N is the number of rows and M is the number of columns of the matrix. Since $M > N$ the problem is ill-posed, i.e. underdetermined. The coefficients A_{ij} are equal to 1 for $i = j$ and equal to -1 for $i = j + \Delta i$. In all other cases $A_{ij} = 0$. Δi is the number of pixels corresponding to the wavelength shift $\Delta \lambda$.

The reconstructed companion spectrum is shown in Fig.10. Note that for display purposes we show it only for the wavelength region covered by the second CRIRES detector in the wavelength setting selected by us. We reconstructed this companion spectrum for the case of a companion mass of $27.11 M_{Jup}$, effective temperature of 2500 K, and rotational velocity of 2 kms⁻¹ (cf. Table 1). As is seen from Fig.10, the main features are reconstructed, but that there are also some discrepancies in the finer details.

Knowing the spectra of the companion several of its parameters can be obtained, such as spectral type of the companion, effective temperature and age.

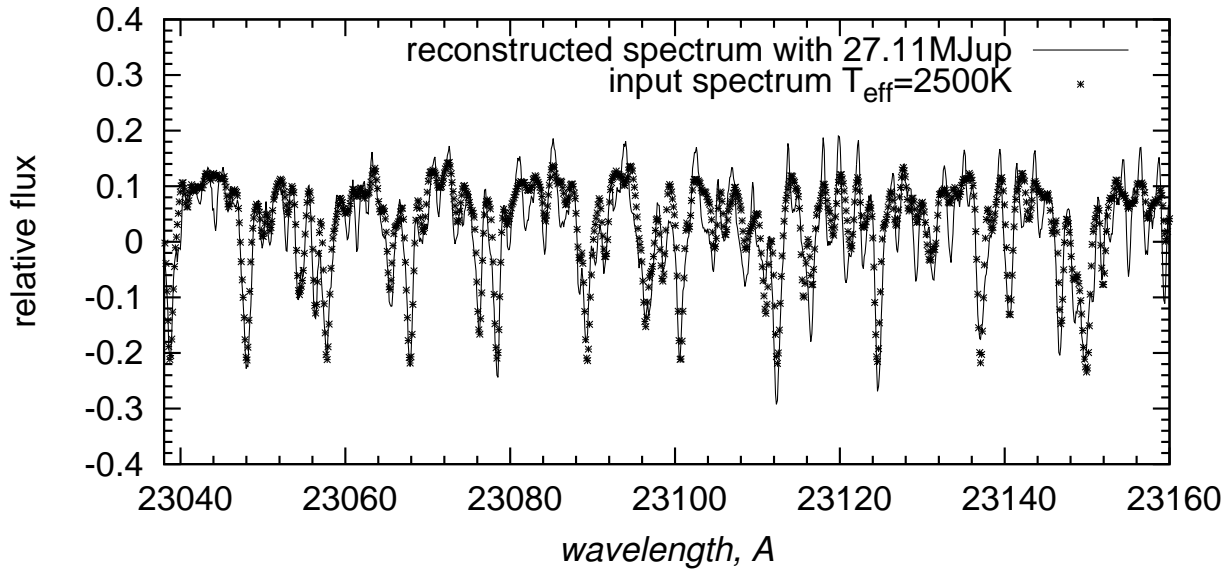


Fig. 10 Companion spectrum (solid line) reconstructed from difference spectrum for a companion with a mass of $27.11 M_{Jup}$. The crosses show the input spectrum of the companion with the same signal-to-noise ratio.

7 Discussion

In recent years a suite of differential observing techniques has been developed which have proven to be very useful tools to discover or characterize sub-stellar companions to stars. An example is spectral differential imaging (Hayden Smith W. 1987, Marois et al. 2000, Lenzen et al. 2003) which employs images taken through different filters in which the companion brightness differs due to a strong spectral feature, but in which the primary star brightness is unchanged. It is essentially by taking the difference of these images that the bright star can be removed, and the companion is uncovered. Another example is angular differential imaging (Marois et al. 2006, Lafrenière et al. 2007, Thalmann et al. 2009) which exploits field rotation in alt-az-mounted telescopes with deactivated derotator (so-called "pupil-tracking mode") to obtain a high fidelity removal of the primary without destruction of the companion signal.

Quite recently, both Rodler et al. (2012) and Brogi et al. (2012) have exploited the CO line region in the K-band that we also use in our study, discovered the spectral signal of the Hot Jupiter companion to τ Boo, and determined its mass. Due to the short orbital period of this system observations from a range of orbital phases were combined. Rodler et al. (2012) used a differential approach for the removal of the stellar spectrum by co-adding all observations into a template that was then subtracted from the individual spectra (for earlier applications of this type of approach see, e.g., Cameron et al. 1999 or Rodler et al. 2010). Brogi et al. (2012) managed to ignore the weak stellar lines of the F7V star in their cross-correlation approach.

In the present paper we provide a differential technique which also employs spectroscopy and leads to the determi-

nation of the RV amplitude and the mass of low-mass and sub-stellar companions to late-type stars with existing orbital solutions for the primary star. Methodologically, our approach bears some resemblance to that taken by Rodler et al. (2012). However, it differs in that we restrict ourselves to the phases of the extrema of the RV curve which is easier to do for objects with longer periods such as GJ1046. Another difference is the application to M dwarfs which have their own strong absorption line system whose removal is more demanding than the treatment of the spectra of earlier-type stars.

While it is the primary goal of our approach to measure the RV amplitude and hence the mass of the companion the fact that we also can approximately reconstruct the companion spectrum is a useful by-product for further characterization of the companion. As can be seen from Fig. 10 the reconstruction is not perfect which is a direct consequence of the fact that we employ only two orbital phases.

In the literature several techniques to uncover the spectra of the companion object in binary star systems have been presented. Simon & Sturm (1994) presented a technique for the disentangling of composite spectra requiring a series of these spectra taken at several orbital phases and, as in our approach, employing singular value decomposition. They applied their method to an O-type binary with components of similar brightness. Hadrava (1995) show how to decompose even the more complex composite spectra of multiple systems in Fourier space. In other work template or model spectra are fitted to remove the primary spectrum and uncover the companion spectrum; see e.g. Griffin & Griffin (2010) who in this case study an F-type companion to a K giant.

The case we present in this paper differs from these literature applications in several respects. First, by restricting the observations to the two phases of the extrema of the binary star RV curve we are attempting to tailor our method to a minimum of observational effort as the planned observations are already very demanding in signal-to-noise ratio, telescope collecting area, and spectral resolution. As we have shown, the CO line region in the K-band provides spectral features narrow enough to measure the RV amplitude of the companion and determine its mass from just the two orbital phases near the RV extrema used to produce the difference spectrum. This works for a wide range of RV amplitudes (corresponding to different orbital inclinations and companion masses). This type of direct measurement would become increasingly difficult (or less precise) due to line blending, if performed in difference spectra obtained from intermediate orbital phases. Since they require spectra from several phases the approaches by Simon & Sturm (1994) or Hadrava (1995) should lead to a better quality of the reconstructed companion spectrum which, in principle, would then also allow the determination of the RV amplitude, provided that the various RV shifts at the different phases can be reconstructed as well with sufficient precision. However, our approach has the advantage of leading to a simple direct measurement that requires the observation of just two selected phases.

Second, we apply our method to M dwarfs which, at the required precision level, do not have fully reliable model spectra and for which it is hard to find fully matching templates. This excludes an approach similar to that adopted by Griffin & Griffin (2010).

Third, the quoted methods from the literature were obviously developed with binary stars in mind whose components do not differ too much in their brightness ratio. This is different in our work which focuses on studying sub-stellar companions that are much fainter than their host stars. Not only do we require very high signal-to-noise ratios, but we also depend on a very good control of systematic effects such as imperfections in the wavelength calibration.

8 Conclusions

In this paper, we have presented a spectral differential technique for the detection and characterization of an invisible close companion to late-type stars. As an example an M2.5V star with a possible brown dwarf companion GJ1046 (Kürster et al. 2008) was chosen. This system is very interesting as it could be the first brown dwarf desert object orbiting around an early-M type star. Only the minimum and maximum mass limits were known from Kürster et al. (2008). The present paper aims at developing a technique to determine the true companion mass.

One of the important parameters for our approach is the star-to-companion brightness ratio. After comparing different wavelength ranges, we have shown that the most suit-

able spectral region to detect the difference spectrum of the companion to GJ1046 is the CO line region in the K-band.

As no high-resolution NIR spectra of GJ1046 are available in the data archives of the relevant observatories, we have simulated CRIRES observations with signal-to-noise ratio equal to 500 in order to study the feasibility for the detection of the companion in the difference spectrum. We show that companion difference spectra with effective temperatures of 2500K, 2000K and 1500K would be possible to detect.

One of the largest sources of systematic error comes from an imperfect wavelength calibration that leads to a mismatch of the shifted stellar spectra before they are subtracted from each other. Our simulations show that the host star spectrum cancels when the mismatch is equal to 0.1 pixels or less.

As rotation of the companion star leads to broadening of the spectral lines that in the difference spectrum can lead to blending of the absorption/pseudoemission features, we have calculated the companion mass for different rotational velocities. We have demonstrated that the determination of the wavelength shift and therefore the companion mass can be made with very high accuracy for slowly rotating companions. Faster rotation of the companion complicates its mass determination, especially for high companion masses.

Our approach of subtracting the primary star spectrum will work, if this spectrum is constant enough. Only in cases of extreme stellar activity may it reach its limit for our test object. We show that the companion difference flux has larger amplitude than the residual signal from the active star unless extreme spot filling factors and spot-to-photosphere temperature differences are assumed.

Knowing the true wavelength shift value we have reconstructed the spectrum using singular value decomposition. From the single (reconstructed) spectrum of the companion, additional parameters can be obtained that give us important information on the companion object.

Acknowledgments

This work was supported by a DAAD stipend to N.M. Kostogryz. M.K. Kuznetsov's work was supported by EU PF7 Marie Curie Initial Training Networks (ITN) ROPACS project (GA N 213646). We thank Pavlenko Ya.V. for his support with the WITA6 programme, F. Rodler for helpful discussions, W. Brandner and anonymous referee for useful comments on our manuscript.

References

- Anders E., Grevesse N., 1989, *Geochim. Cosmochim. Acta*, 53, 197
- Allard F., Hauschildt P.H., Alexander D.R., et al., 2001, *ApJ*, 556, 357
- Barber R.J., Tennyson J., Harris G.J., Tolchenov R., 2006, *MNRAS*, 368, 1087

- Brogi M., Snellen I.A.G., de Kok R.J., Albrecht S., Birkby J., de Mooij E.J.W., 2012, *Nature*, 486, 502
- Burrows A., Ram S. R., Bernath P., 2002, *ApJ*, 577, 986
- Claret, A.; Bloemen, S., 2011, *A&A*, 529, A75
- Clough S.A., Iacono M.J. and Moncet J.-L., 1992, *J. Geophys. Res.*, 97, 15761
- Clough S.A. and Iacono M.J., 1995, *J. Geophys. Res.*, 100, 16519
- Clough S.A., Shephard M.W., Mlawer E.J., Delamere J.S., Iacono M.J. et al., 2005, *JQSRT*, 91, 233
- Cochran W.D., Hatzes A.P., and Hancock T.J., 1991, *ApJ*, 380, L35
- Collier Cameron A., Horne K., Penny A., James D., 1999, *Nature*, 402, 751
- Deleuil M., Deeg H.J., Alonso R., et al., 2008, *A&A*, 491, 889
- Endl M., Hatzes A.P., Cochran W.D., et al., 2004, *ApJ*, 611, 1121
- Goorvitch D., 1994, *ApJS*, 95, 535
- Gray D.F., 1976, *The observation and analysis of stellar photospheres* (New York: Wiley-Interscience), 484
- Grether D. and Lineweaver C.H., 2006, *ApJ*, 640, 1051
- Griffin R.E.M., Griffin R.F., 2010, *MNRAS*, 402, 1675
- Hadrava P., 1995, *A&A Suppl. Ser.*, 114, 393
- Hayden Smith W., 1987, *PASP*, 99, 1344
- Jenkins J.S., Jones H.R.A., Goździewski K., 2009, *MNRAS*, 398, 911
- Klahr H., Brandner W., 2006, *Planet Formation: Theory, Observations, and Experiments* (Cambridge: University Press) ISBN 0521860156
- Knapp G.R., Leggett S.K., Fan X., Marley M.S., Geballe T.R., et al., 2004, *AJ*, 127, 3553
- Kupka F., Piskunov N.E., Ryabchikova T.A., Stempels H.C., Weiss W.W., 1999, *A&AS*, 138, 119
- Kürster M., Endl, M., Reffert, S., 2008, *A&A*, 483, 869
- Lafrenière D., Marois C., Doyon R., Nadeau D., Artigau É., 2007, *ApJ*, 660, 770
- Latham D.W., Mazeh T., Stefanik R.P., et al., 1989, *Nature*, 339, 38
- Lee B.L., Ge J., Fleming S.W., et al., 2011, *ApJ*, 728, 32
- Lenzen, R., Hartung M., Brandner W., Finger G., Hubin N.N., et al., 2003, *Proc. SPIE*, 4841, 994
- Marcy G.W., Butler R.P., Vogt S.S., et al., 2001, *ApJ*, 555, 418
- Marois C., Doyon R., Racine R., Nadeau D., 2000, *PASP*, 112, 91
- Marois C., Lafrenière D., Doyon R., Macintosh B., Nadeau D., 2006, *ApJ*, 641, 556
- Marquardt D.W., 1963, *Journal of the Society for industrial and Applied Mathematics*, 11, 431
- Mazeh T., Latham D.W., and Stefanik R.P., 1996, *ApJ*, 446, 415
- Montagnier G., Ségransan D., Beuzit J.-L., et al., 2006, *A&A*, 460, L19
- Nidever D.L., Marcy G.W., Butler R.P., et al., 2002, *ApJS*, 141, 503N
- O'Neal D., Neff J.E., Saar S.H., & Mines J.K., 2001, *AJ*, 122, 1954
- O'Neal D., Neff J.E., Saar S.H., & Cuntz M., 2004, *AJ*, 128, 1802
- Pavlenko, Ya., 2000, *Astron. Rept*, 44, 219
- Pavlenko, Ya., Zapatero Osorio, M.R., Rebolo, R., 2000, *A&A*, 355, 245
- Press W.H., Teukolsky S.A., Vetterling W.T., Flannery B.P., 1992, *Numerical recipes in C. The art of scientific computing* (Cambridge: University Press)
- Reiners A., Bean J.L., Huber K.F., et al. 2010, *ApJ*, 710, 432
- Rodler F., Kürster M., Henning T., 2010, *A&A*, 514, 23
- Rodler F., Lopez-Morales M., and Ribas I., 2012, *ApJ*, 753, 25
- Rothman L.S., Gordon I.E., Barbe A., Benner D.C., Bernath P.F. et al., 2009, *JQSRT*, 110, 533
- Scholz A., Eisloffel J., Froebrich D., 2005, *A&A*, 438, 675
- Seifahrt A., Käufel H.U., Zängl G., Bean J.L., Richter M.J., Siebenmorgen R., 2010, *A&A*, 524, 23
- Simon K.P., Sturm E., 1994, *A&A*, 281, 286
- Solanki S.K., 2003, *A&AR*, 11, 153
- Stamatellos D., Whitworth A.P., 2009, *MNRAS*, 392, 413
- Testi L., 2009, *A&A*, 503, 639
- Thalmann C., Carson J., Janson M., Goto M., McElwain M., 2009, *ApJ*, 707, L123
- Terndrup D.M., Krishnamurthi A., Pinsonneault M.H., Stauffer J.R., 1999, *AJ*, 118, 1814
- Udry S., Mayor M., Naef D., et al., 2002, *A&A*, 390, 267
- Zechmeister M., Kürster M., Endl M., 2009, *A&A*, 505, 859